Application of Moving Kriging Shape Functions on Plate Problems

Shazim Ali Memon*, Worsak Kanok-Nukulchai, Sajjad Haider***
*National Institute of Transportation
National University of Sciences and Technology, Islamabad, Pakistan
shazim_memon@yahoo.com
**School of Civil Engineering,
Asian Institute of Technology, Pathumthani, 12120, Thailand

Abstract

The Moving Kriging (MK) interpolation was recently proposed as a superior substitution of the Moving Least Square (MLS) approximation in the construction of shape functions for the Element-Free Galerkin Method (EFGM). Although Kriging is already a very well-known geostatistical technique for spatial interpolation in geology and mining, it has only been applied recently in computational mechanics. This paper presents an improved version of the EFGM based on the MK interpolation for addressing the problems of shear locking in Mindlin plates at the small thickness limit. Numerical results show that the modified version of EFGM with MK interpolation does not exhibit shear locking. Furthermore, the study also finds the accuracy of EFGM to be greatly enhanced with the use of MK shape functions.

Key words: Moving Kriging Interpolation, Element-Free Galerkin Method, Moving Least Square Approximation, Shear Locking, Mindlin Plates

Introduction

In recent years, EFGM proposed by Belytschko et al. [1] has found many applications [2]. The EFGM commonly employs shape functions constructed from a MLS approximation which was formally introduced and studied by Lancaster and Salkauskas [3]. The MLS approximation has two major features that make it popular: 1) the approximated field function is continuous and smooth in the entire problem domain; and 2) it is capable of producing an approximation with the desired order of consistency. The key disadvantage of MLS approximation is its interpolation property that does not allows exact imposition of essential boundary conditions. In other words, MLS approximations lack the delta function property possessed by finite element shape functions.

The MK interpolation was recently proposed as a superior substitution of the MLS approximation in the construction of shape functions for the EFGM. Although Kriging is already a very well-known geostatistical technique for spatial interpolation in geology and mining, it has only been applied recently in computational mechanics. The key advantage of the MK interpolation is its interpolation property that allows exact imposition of essential boundary conditions, similar to the conventional Finite Element Method (FEM). In fact with the MK shape functions, EFGM using finite elements as integration cells can be viewed as a class of FEM that employ element-free shape functions, e.g., the shape functions untied to the element structure [4].

It has long been recognized that the shear locking phenomenon results from an inconsistency between the rotation and the transverse displacement fields. To prevent shear locking, the interpolation field for rotation must have the built-in capability to match the corresponding first derivative of the transverse displacement field. With regards to the FEM, this match can generally be arranged for one-dimensional bending elements [5]. However, in 2D finite elements such as plates and shells, such consistency may not be possible since the shape functions are generally constrained by the element nodal structure. It is then imperative to provide some linkage between the definition of the rotation and transverse displacement fields so that Kifchhoff's constraints may be satisfied approximately.

In the framework of meshless methods [6], the complexity in constructing consistent shape functions, as hampered by the element nodal structure, no longer exists. This is a remarkable advantage of meshless approaches since it allows the definition of smooth and consistent approximations of rotations and displacements. Donning and Liu [7] first noted this exceptional benefit in addressing the problem of transverse shear locking in Mindlin type bending elements. Recognizing the potential of the matching fields approach outlined in the work of Donning and Liu [7], it is applied herein, in conjunction with the EFGM. With this strategy, slope and normal rotation in each direction are more than field consistent; they built with a capacity to perfectly match each other at the outset and therefore satisfy the zero shear strain at the thin limits. This leads to a complete absence of transverse shear locking and thus a high degree of accuracy of EFGM analyses employing either uniform or non-uniform nodal arrangements, regardless of the slenderness ratio of the respective plates.

Corresponding Author: Shazim Ali Memon
NUST Publishing, © (2008), ISSN: 2070-9900

Moving kriging interpolation and the concept of domain of influence

In Moving Kriging, the approximation u(x) is defined as

$$u^h(\mathbf{x}) = \sum_{j=1}^{m} p_j(\mathbf{x}) a_j + \mathrm{Z}(\mathbf{x}) \quad (1)$$

Where

$\sum_{j=1}^{m} p_j(\mathbf{x}) a_j$ is polynomial basis function with m order

$\mathrm{Z}(\mathbf{x})$ is a stochastic parameter which creates localized deviation from interpolation of n sampling points.

The covariance of Z(x) is defined by the correlation of n sampling points or n nodes called the correlation matrix

$$\mathrm{R}[\mathrm{R}(x_i.x_j)] \quad (2)$$

The element of correlation matrix is the correlation function in the form of a Gaussian function as,

$$\mathrm{R}(\mathrm{x_i}, \mathrm{x_j}) = e^{-\left(\frac{r_{ij}}{\alpha d_m}\right)^2}, \qquad d_m = \frac{1}{n}\sum_{k}^{n} d_{mk} \quad (3)$$

Where

r_{ij}/d_m is distance between 2 nodes normalized to Domain Of Influence (DOI), its magnitude does not depends on the unit used.

α is non-unit parameter after r_{ij} is normalized by the size of DOI.

d_{mk}=Domain of influence of each node at x_k

Figures 1-2 schematically illustrates the concept of the DOI of a node and the concept of the domain of nodal visibility of all numerical integration points in an element respectively [4, 8, and 9].

Shear locking

In FEM, the use of element-tied shape functions create shear locking problems in shear deformable plate elements due to the incompatibility between rotations and transverse displacement. In EFGM, shear locking problem has been eliminated by adopting the field-matching strategy [10 and 11].

For Mindlin plates, the approximate fields for the transverse displacement and the two rotations can be expressed as:

$$w^h(x, y) = \sum_{I=1}^{n} \varphi_I(x, y) w_I \quad (4)$$

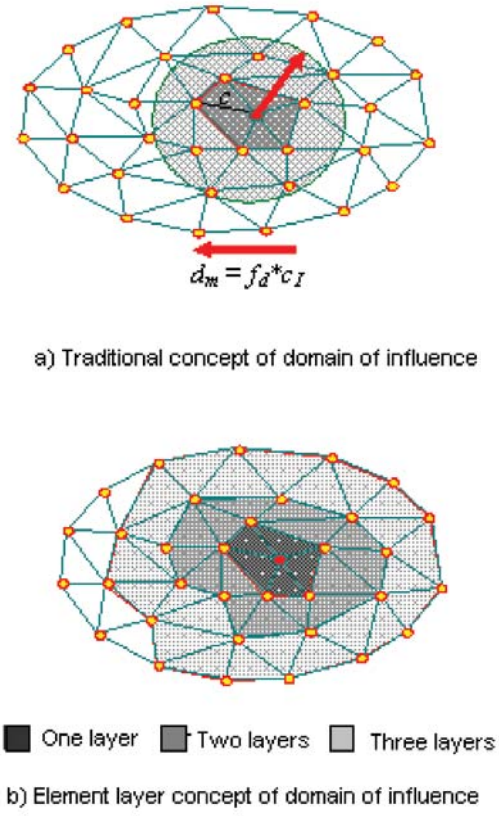

Fig. 1. Domain of influence concepts of a nodal point

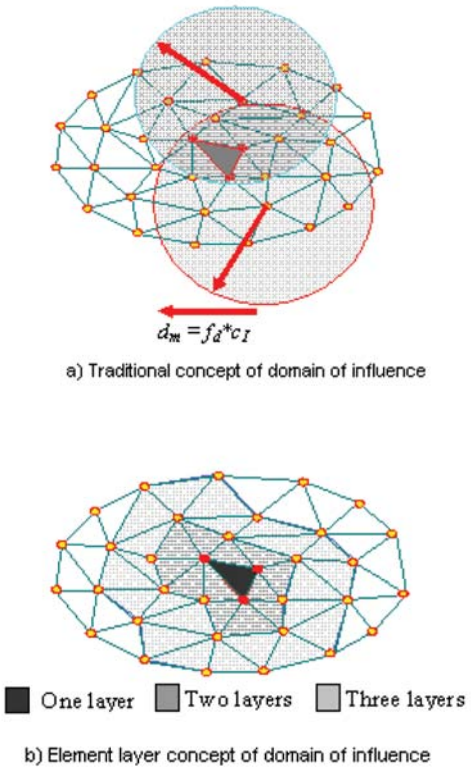

Fig. 2. Domain of influence concepts of an element

$$\theta_x^h(x,y)=\sum_{I=1}^{n}\eta_I(x,y)\theta_{xI} \tag{5}$$

$$\theta_y^h(x,y)=\sum_{I=1}^{n}\xi_I(x,y)\theta_{yI} \tag{6}$$

where $\varphi_I(x,y)$ denotes a shape function for approximating transverse displacement, $\eta_I(x,y)$ is a shape function for approximating rotations in the *x*-direction, and $\xi_I(x,y)$ is a shape function for approximating rotations in the *y*-direction. $\varphi_I(x,y)$ is shape function based on MK interpolation, while $\eta_I(x,y)$ and $\xi_I(x,y)$ are directly derived from the partial derivative of $\varphi_I(x,y)$ as

$$\begin{aligned}\eta_I(x,y)&=\frac{\partial}{\partial x}\varphi_I(x,y)\ \text{ and}\\ \xi_I(x,y)&=\frac{\partial}{\partial y}\varphi_I(x,y)\end{aligned} \tag{7}$$

Element-free galerkin formulation for Mindlin plates

Modeling

The two dimensional Mindlin plate model possesses three independent variables at the middle surface of the plate. After the plate is loaded, two basic assumptions are made: 1) the transverse strain is neglected; 2) plane sections remain plane but not necessarily normal to the neutral axis. For Mindlin plate, we have the following relations

$$\theta_x(x,y)=u_x(x,y)-\gamma_{xz}(x,y) \tag{8}$$

$$\theta_y(x,y)=u_y(x,y)-\gamma_{yz}(x,y) \tag{9}$$

In which u(x,y) is the transverse displacement; $\theta_x(x,y)$and $\theta_y(x,y)$ represent rotations of normal to the mid-surface in the x- and y-directions respectively; and $\gamma_{xz}(x,y)$ and $\gamma_{yz}(x,y)$ denote equivalent constant shearing strains in the z-direction on planes which are normal to the x- and y-axes respectively.

Total potential energy

The total potential energy of Mindlin plate is given by

$$\begin{aligned}\Pi(u,\theta_x,\theta_y)&=U_b(\theta_x,\theta_y)+\\ &U_s(u,\theta_x,\theta_y)-\Omega(u,\theta_x,\theta_y)\end{aligned} \tag{10}$$

where,

$$\begin{aligned}U_b(\theta_x,\theta_y)=\frac{1}{2}\int D_b\Big[&\theta^2{}_{x,x}+\theta^2{}_{y,y}+2\nu\theta_{x,x}\theta_{y,y}+\\ &\left(\frac{1-\nu}{2}\right)(\theta_{x,y}+\theta_{y,x})\Big]dA\end{aligned} \tag{11}$$

$$\begin{aligned}&U_s(u,\theta_x,\theta_y)=\\ &\frac{1}{2}\int D_S\begin{bmatrix}(u,_x-\theta_x)^2+\\ (u,_y-\theta_y)^2\end{bmatrix}dA\end{aligned} \tag{12}$$

For the problem subjected to a distributed transverse load,

$$\Omega(u)=\int q_u u dA \tag{13}$$

Hence, the total potential energy can be further expressed as

$$\begin{aligned}&\Pi(u,\theta_x,\theta_y)=\\ &\frac{1}{2}\int D_b\begin{bmatrix}\theta^2{}_{x,x}+\theta^2{}_{y,y}+2\nu\theta_{x,x}\theta_{y,y}+\\ \left(\frac{1-\nu}{2}\right)(\theta_{x,y}+\theta_{y,x})\end{bmatrix}dA\\ &+\frac{1}{2}\int D_S\begin{bmatrix}(u,_x-\theta_x)^2+\\ (u,_y-\theta_y)^2\end{bmatrix}dA-\int q_u u dA\end{aligned} \tag{14}$$

The first variation of equation (11) yields

$$\delta\Pi(u,\theta_x,\theta_y)=\delta U_b+\delta U_s-\delta\Omega=0 \tag{15}$$

Formulation of the Galerkin discretized equations for Mindlin plates

Unlike EFGM, consistent shape functions for the displacement field and rotation field are adopted here to avoid shear locking. The unknown functions of the problem can be approximated as:

$$u(x,y)=\sum_n \varphi^n u^n=\{\varphi\}^T\{u\} \tag{16a}$$

$$\theta_x(x,y)=\sum_n \eta^n\theta_x{}^n=\{\eta\}^T\{\theta_x\} \tag{16b}$$

$$\theta_y(x,y)=\sum_n \xi^n\theta_y{}^n=\{\xi\}^T\{\theta_y\} \tag{16c}$$

$$w_u(x,y)=\sum_n \varphi^n w_u{}^n=\{\varphi\}^T\{w_u\} \tag{16d}$$

$$w_{\theta_x}(x,y)=\sum_n \eta^n w_{\theta_x}{}^n=\{\eta\}^T\{w_{\theta_x}\} \tag{16e}$$

$$w_{\theta_y}(x,y)=\sum_n \xi^n w_{\theta_y}{}^n=\{\xi\}^T\{w_{\theta_y}\} \tag{16f}$$

In which {η} is a vector of shape functions for rotation field in the x-direction computed from the first partial x-derivative of {φ} and {ξ} is a vector of shape functions for the rotation field in y-direction computed from the first partial y-derivative of {φ}.

From equation (15) and (16), the first Galerkin equation can be formulated as shown below:

$$G_u = -\int q_u u dA - \int D_S \begin{bmatrix} (u_{,xx} + u_{,yy}) - \\ (\theta_{x,x} + \theta_{y,y}) \end{bmatrix} w_u dA + \text{boundary terms} \quad (17)$$

Taking integration by parts leads to

$$G_u = \int D_S \begin{bmatrix} (u_{,x} - \theta_{,x}) w_{u,x} + \\ (u_{,y} - \theta_{,y}) w_{u,y} \end{bmatrix} dA - \int q_u w_u dA \quad (18)$$

Substituting approximation functions from equations (16a)-(16f) into equation (18) yields

$$G_u = \int D_s \begin{pmatrix} \{\varphi_{,x}\}\{u\}\{\varphi_{,x}\} - \{\eta\}\{\theta_x\}\{\varphi_{,x}\} + \\ \{\varphi_{,y}\}\{u\}\{\varphi_{,y}\} - \{\xi\}\{\theta_y\}\{\varphi_{,y}\} \end{pmatrix} \{w_u\} + \int q_u \{\varphi\}\{w_u\} dA \quad (19)$$

$$G_u = \{w_u\}^T \begin{bmatrix} \left(\int D_s \begin{pmatrix} \{\varphi_{,x}\}^T \{\varphi_{,x}\} + \\ \{\varphi_{,y}\}^T \{\varphi_{,y}\} \end{pmatrix} dA \right) \{u\} - \\ \left(\int D_s \{\varphi_{,x}\}^T \{\eta\} dA \right) \{\theta_x\} \\ - \left(\int D_s \{\varphi_{,y}\}^T \{\xi\} dA \right) \{\theta_y\} - \\ \int \{\varphi\}^t q_u dA \end{bmatrix} \quad (20)$$

Arbitrary variations of $\{w_u\}$ lead to the following equation in matrix form

$$[K_u]_1 \{u\} + [K_{\theta_x}]_1 \{\theta_x\} + [K_{\theta_y}]_1 \{\theta_y\} = \{R_u\} \quad (21)$$

where

$$[K_u]_1 = \int D_s \left(\{\varphi_{,x}\}^T \{\varphi_{,x}\} + \{\varphi_{,y}\}^T \{\varphi_{,y}\} \right) dA$$

$$[K_{\theta_x}]_1 = -\int D_s \{\varphi_{,x}\}^T \{\eta\} dA$$

$$[K_{\theta_y}]_1 = -\int D_s \{\varphi_{,y}\}^T \{\xi\} dA$$

and $\{R_u\} = \int \{\varphi\}^t q_u dA$

In the same manner

$$G_{\theta x} = -\int D_b \begin{bmatrix} \theta_{x,xx} + \left(\frac{1+\nu}{2} \right) \theta_{y,xy} + \\ \left(\frac{1-\nu}{2} \right) \theta_{x,yy} \end{bmatrix} w_{\theta x} dA + \int D_s (\theta_x - u_{,x}) w_{\theta x} dA + \text{boundary terms} \quad (22)$$

$$G_{\theta x} = \int D_b \begin{bmatrix} \theta_{x,x} w_{\theta x} + \nu \theta_{y,y} w_{\theta x,x} + \\ \left(\frac{1-\nu}{2} \right) \theta_{x,y} w_{\theta x,y} + \left(\frac{1-\nu}{2} \right) \theta_{y,x} w_{\theta x,y} \end{bmatrix} dA + \int D_s (\theta_x - u_{,x}) w_{\theta x} dA \quad (23)$$

$$G_{\theta x} = \{w_{\theta x}\}^T \begin{bmatrix} -\left(\int D_S \{\eta\}^T \{\varphi_{,x}\} dA \right) \{u\} + \\ \left(\int \begin{pmatrix} D_S \begin{pmatrix} \{\eta_{,x}\}^T \{\eta_{,x}\} + \\ \left(\frac{1-\nu}{2} \right) \{\eta_{,y}\}^T \{\eta_{,y}\} \end{pmatrix} + \\ D_S{}^T \{\eta\}^T \{\eta\} \end{pmatrix} dA \right) \{\theta_x\} \\ + \left(\int D_b \begin{pmatrix} \nu \{\eta_{,x}\}^T \{\xi_{,y}\} + \left(\frac{1-\nu}{2} \right) \\ \{\eta_{,y}\}^T \{\xi_{,x}\} \end{pmatrix} dA \right) \{\theta_y\} \end{bmatrix} \quad (24)$$

Arbitrary variations of $\{w_u\}$ lead to the following equation in matrix form

$$[K_u]_2 \{u\} + [K_{\theta_x}]_2 \{\theta_x\} + [K_{\theta_y}]_2 \{\theta_y\} = \{R_{\theta_x}\} \quad (25)$$

where

$$[K_u]_2 = -\int D_s \{\eta\}^T \{\varphi_{,x}\}^T dA$$

$$[K_{\theta_x}]_2 = \int \begin{pmatrix} D_s \begin{pmatrix} \{\eta_{,x}\}^T \{\eta_{,x}\} + \\ \left(\frac{1-\nu}{2} \right) \{\eta_{,y}\}^T \{\eta_{,y}\} \end{pmatrix} + \\ D_s{}^T \{\eta\}^T \{\eta\} \end{pmatrix} dA$$

$$[K_{\theta_y}]_2 = \int D_b \begin{pmatrix} \nu \{\eta_{,x}\}^T \{\xi_{,y}\} + \\ \left(\frac{1-\nu}{2} \right) \{\eta_{,y}\}^T \{\xi_{,x}\} \end{pmatrix} dA \text{ and } \{R_{\theta_x}\} = \{0\}$$

Similarly,

$$G_{\theta_y} = -\int D_b \left[\begin{array}{l} \theta_{y,yy} + \left(\frac{1+\nu}{2}\right)\theta_{x,xy} \\ + \left(\frac{1-\nu}{2}\right)\theta_{y,xx} \end{array} \right] w_{\theta_y} dA + \int D_s \left(\theta_y - u_{,y}\right) w_{\theta_y} dA + \text{boundary terms} \quad (26)$$

$$G_{\theta_y} = \int D_b \left[\begin{array}{l} \theta_{y,y} w_{\theta_y,y} + \nu\theta_{x,x} w_{\theta_y,y} + \\ \left(\frac{1-\nu}{2}\right)\theta_{y,x} w_{\theta_y,x} + \left(\frac{1-\nu}{2}\right)\theta_{x,y} w_{\theta_y,x} \end{array} \right] dA + \int D_s \left(\theta_y - u_{,y}\right) w_{\theta_y} dA \quad (27)$$

$$G_{\theta_y} = \int D_b \left(\begin{array}{l} \{\xi_{,y}\}\{\theta_y\}\{\xi_{,y}\} + \\ \nu\{\eta_{,x}\}\{\theta_x\}\{\xi_{,y}\} + \\ \left(\frac{1-\nu}{2}\right)\{\eta_{,y}\}\{\theta_x\}\{\xi_{,x}\} + \\ \left(\frac{1-\nu}{2}\right)\{\xi_{,x}\}\{\theta_y\}\{\xi_{,x}\} \end{array} \right) \{w_{\theta_y}\} dA + \int D_s \left(\{\xi\}\{\theta_y\}\{\xi\} - \{\varphi_{,y}\}\{u\}\{\xi\} \right) \{w_{\theta_y}\} dA \quad (28)$$

$$G_{\theta_y} = \{w_{\theta_y}\}^T \left[\begin{array}{l} -\left(\int D_s \{\xi\}^T \{\varphi_{,y}\} dA\right)\{u\} + \\ \left(\int D_b \{\xi_{,y}\}^T \{\eta_{,x}\} + \left(\frac{1-\nu}{2}\right)\{\xi_{,x}\}^T \{\eta_{,y}\} dA \right)\{\theta_x\} \\ + \int \left(\begin{array}{l} D_s \{\xi\}^T \{\xi\} + D_b \\ \left(\{\xi_{,y}\}^T \{\xi_{,y}\} + \left(\frac{1-\nu}{2}\right)\{\xi_{,x}\}^T \{\xi_{,x}\} \right) \end{array} \right) dA \{\theta_y\} \end{array} \right] \quad (29)$$

Arbitrary variations of $\{w_u\}$ lead to the following equation in matrix form

$$\begin{array}{l} [K_u]_3\{u\} + [K_{\theta_x}]_3\{\theta_x\} + \\ [K_{\theta_y}]_3\{\theta_y\} = \{R_{\theta_Y}\} \end{array} \quad (30)$$

where

$$[K_u]_3 = -\int D_s \{\xi\}^T \{\varphi_{,y}\} dA$$

$$[K_{\theta_x}]_3 = \int D_b \{\xi_{,y}\}^T \{\eta_{,x}\} + \left(\frac{1-\nu}{2}\right)\{\xi_{,x}\}^T \{\eta_{,y}\} dA$$

$$[K_{\theta_y}]_3 = \int \left(\begin{array}{l} D_s \{\xi\}^T \{\xi\} + D_b \\ \left(\{\xi_{,y}\}^T \{\xi_{,y}\} + \left(\frac{1-\nu}{2}\right)\{\xi_{,x}\}^T \{\xi_{,x}\} \right) \end{array} \right) dA$$

and $\{R_{\theta_y}\} = \{0\}$

Equation (21), (25), and (30) can be combined into the following matrix form:

$$\left[\begin{array}{ccc} [K_u]_1 & [K_{\theta_x}]_1 & [K_{\theta_y}]_1 \\ [K_u]_2 & [K_{\theta_x}]_2 & [K_{\theta_y}]_2 \\ [K_u]_3 & [K_{\theta_x}]_3 & [K_{\theta_y}]_3 \end{array} \right] \left[\begin{array}{c} \{u\} \\ \{\theta_x\} \\ \{\theta_y\} \end{array} \right] = \left[\begin{array}{c} \{R_u\} \\ \{R_{\theta_x}\} \\ \{R_{\theta_Y}\} \end{array} \right] \quad (31)$$

The above expression formulation in equation (31) is for Mindlin plates under distributed transverse load. A more general formulation is shown in Table 1.

Numerical investigation

Application of EFGM based on MK shape functions to Mindlin plates is addressed. Following notations are used to identify boundary and loading types: SS-C for simply supported plate under center point load and CL-C for clamped plate under center point load. The full square plate is discretized by seven nodes uniformly spaced in each direction and 6 x 6 regular background cells are constructed as shown in Figure 3. The following properties of plates are used: square plate width L=10, thickness D=0.1, E=30x10^6, Poisson's ratio η=0.3 and shear correction factor k=5/6. For SS-C and CL-C point load of magnitude 40 is applied.

Table 1. Linear Discretized Equations for General Case of Mindlin Plates

$$[K_b + K_s][u] = [\mathrm{R}]$$

$$\begin{bmatrix} \int D_s\left(\{\varphi,_x\}^T\{\varphi,_x\}+\{\varphi,_y\}^T\{\varphi,_y\}\right)dA & -\int D_s\{\varphi,_x\}^T\{\eta\}dA & -\int D_s\{\varphi,_y\}^T\{\xi\}dA \\ -\int D_s\{\eta\}^T\{\varphi,_x\}^T dA & \int\left(D_s\left(\{\eta,_x\}^T\{\eta,_x\}+\left(\frac{1-\nu}{2}\right)\{\eta,_y\}^T\{\eta,_y\}\right)+D_s{}^T\{\eta\}^T\{\eta\}\right)dA & \int D_b\left(\nu\{\eta,_x\}^T\{\xi,_y\}+\left(\frac{1-\nu}{2}\right)\{\eta,_y\}^T\{\xi,_x\}\right)dA \\ -\int D_s\{\xi\}^T\{\varphi,_y\}dA & \int D_b\{\xi,_y\}^T\{\eta,_x\}+\left(\frac{1-\nu}{2}\right)\{\xi,_x\}^T\{\eta,_y\}dA & \int\left(D_s\{\xi\}^T\{\xi\}+D_b\left(\{\xi,_y\}^T\{\xi,_y\}+\left(\frac{1-\nu}{2}\right)\{\xi,_x\}^T\{\xi,_x\}\right)\right)dA \end{bmatrix}$$

in which additional symbols are defined as follows:

$q_{\theta x}$ = external moment (in x - direction)

$q_{\theta y}$ = external moment (in y - direction)

t_u = external traction force along Γ_u^n

$t_{\theta x}$ = external traction moment (in x - direction) along $\Gamma_{\theta x}^n$

$t_{\theta y}$ = external traction moment (in y - direction) along $\Gamma_{\theta y}^n$

Γ_u^n = a natural boundary for transverse displaceme nt field

$\Gamma_{\theta x}^n$ = a natural boundary for rotation (in x - direction) field

$\Gamma_{\theta y}^n$ = a natural boundary for rotation (in y - direction) field

$$\begin{bmatrix} \{u\} \\ \{\theta_x\} \\ \{\theta_y\} \end{bmatrix} = \begin{bmatrix} \int\{\varphi\}^T q_u dA+\int\{\varphi\}^T t_u d\Gamma_u^n \\ \int\{\eta\}^T q_{\theta_x} dA+\int\{\eta\}^T t_{\theta_x} d\Gamma_{\theta_x}^n \\ \int\{\varepsilon\}^T q_{\theta_y} dA+\int\{\varepsilon\}^T t_{\theta_y} d\Gamma_{\theta_y}^n \end{bmatrix}$$

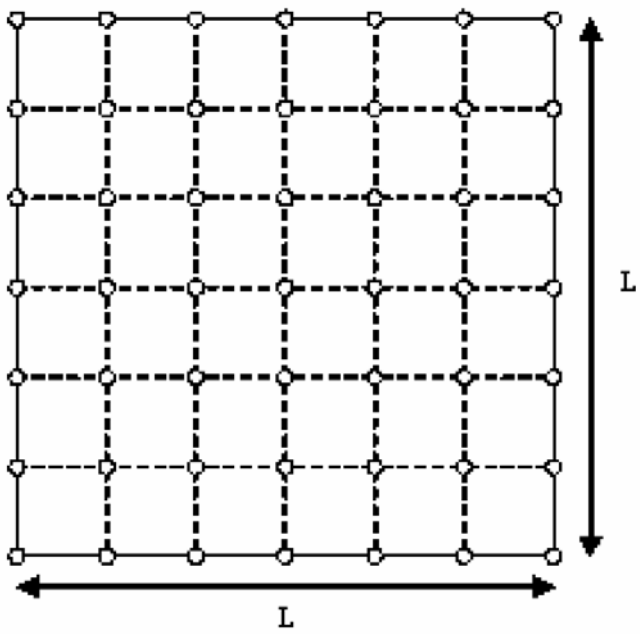

Fig. 3. Arrangement of nodal structure for full square plate using uniform Element Free Galerkin (EFG) discretization and regular background cell structure equivalent to Finite Element mesh

Investigation of quadrature scheme

Quadrature scheme is investigated first for this improved version of EFGM since it affects the accuracy and the computational time. Results of normalized center displacement with respect to exact solution vs. number of monomial terms in the polynomial function are plotted in Figures 4-13 for various quadrature schemes. Test results reveal that the difference of accuracy between 6 x 6 and 8 x 8 quadrature schemes is rather insignificant. Therefore, based on accuracy and computational cost 6 x 6 integration scheme is adopted.

Investigation of domain of influence

Results of normalized center displacement with respect to exact solution vs. number of monomial terms in the polynomial function are plotted in Figures 4-13 for various quadrature schemes. Numerical results in graphical format reveal that the radius of DOI must be large enough to cover n_p layers of cells surrounding the associated node, where n_p is the order of basis function, to maintain adequate numerical conditioning of system. This statement is in agreement with the theory proposed by Kanok-Nukulchai et al. [12].

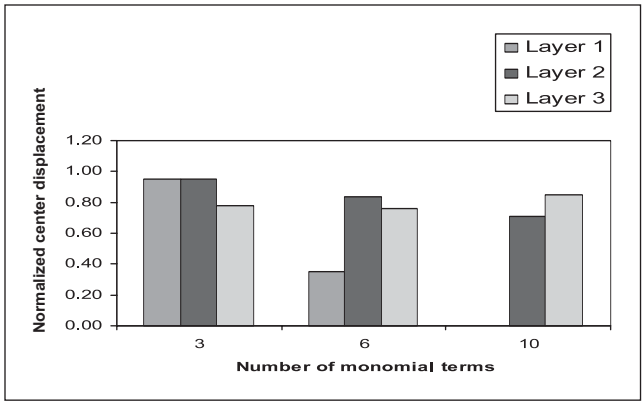

Fig. 4. SS-C thin square plate (L/D=100): normalized center displacement vs. number of monomial terms in the basis function having quadrature rule 4 x 4 for various domain of influence

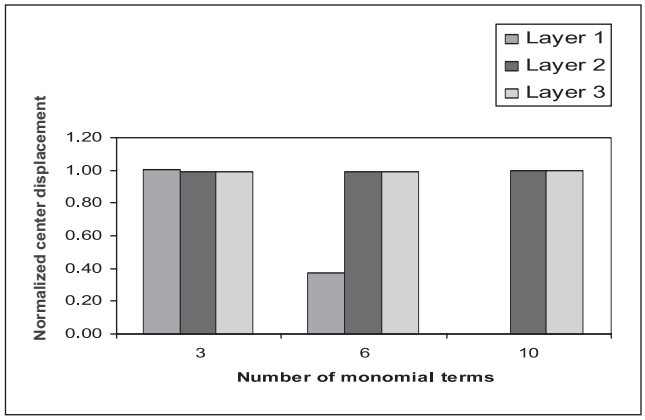

Fig. 7. SS-C thin square plate (L/D=100): normalized center displacement vs. number of monomial terms in the basis function having quadrature rule 7 x 7 for various domain of influence

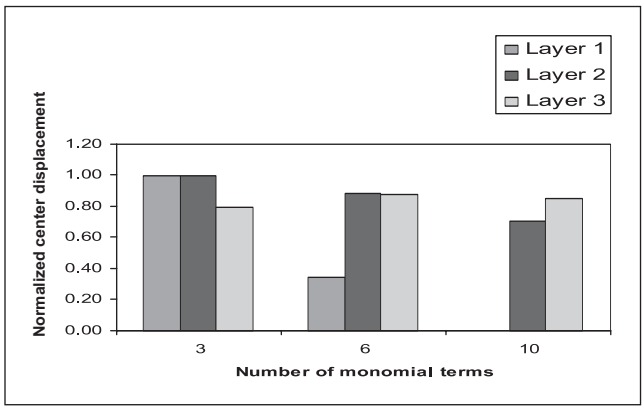

Fig. 5. SS-C thin square plate (L/D=100): normalized center displacement vs. number of monomial terms in the basis function having quadrature rule 5 x 5 for various domain of influence

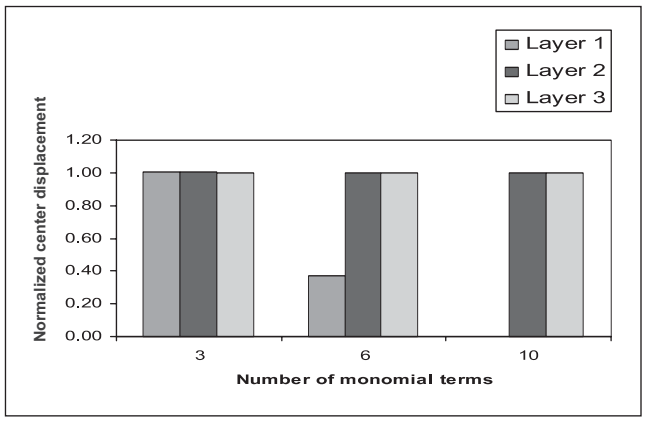

Fig. 8. SS-C thin square plate (L/D=100): normalized center displacement vs. number of monomial terms in the basis function having quadrature rule 8 x 8 for various domain of influence

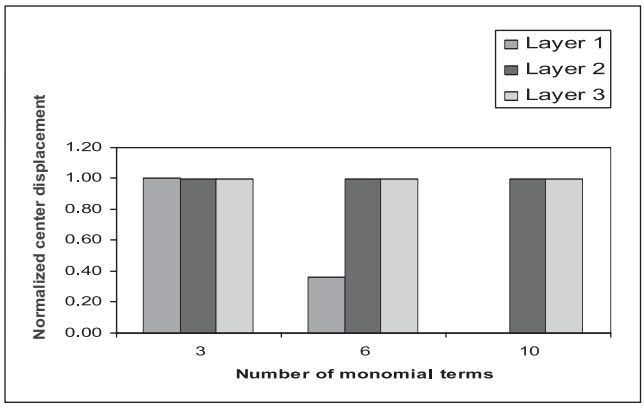

Fig. 6. SS-C thin square plate (L/D=100): normalized center displacement vs. number of monomial terms in the basis function having quadrature rule 6 x 6 for various domain of influence

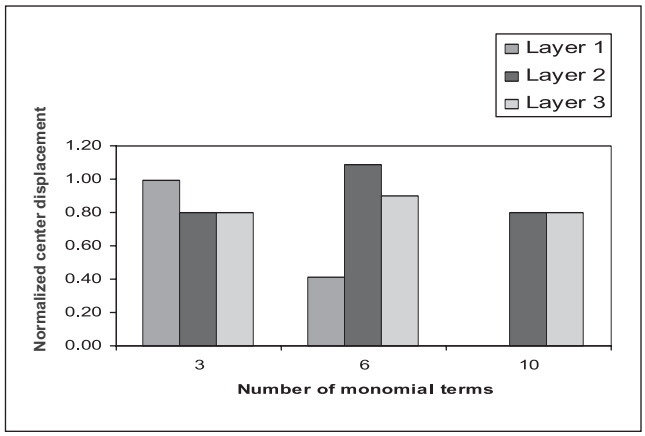

Fig. 9. CL-C thin square plate (L/D=100): normalized center displacement vs. number of monomial terms in the basis function having quadrature rule 4 x 4 for various domain of influence

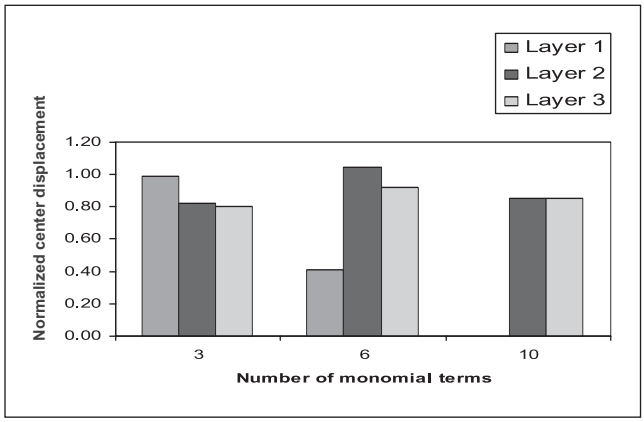

Fig. 10. CL-C thin square plate (L/D=100): normalized center displacement vs. number of monomial terms in the basis function having quadrature rule 5 x 5 for various domain of influence

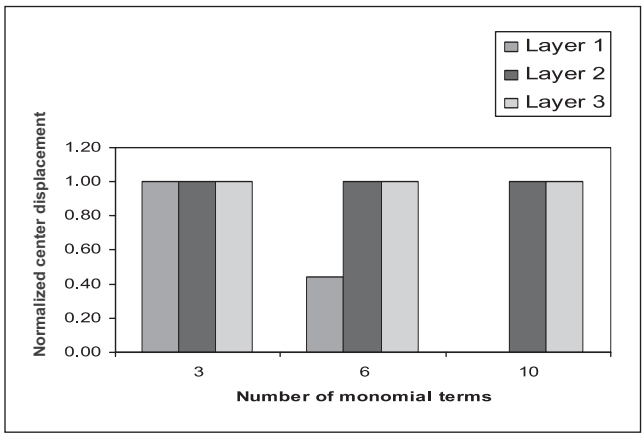

Fig. 11. CL-C thin square plate (L/D=100): normalized center displacement vs. number of monomial terms in the basis function having quadrature rule 6 x 6 for various domain of influence

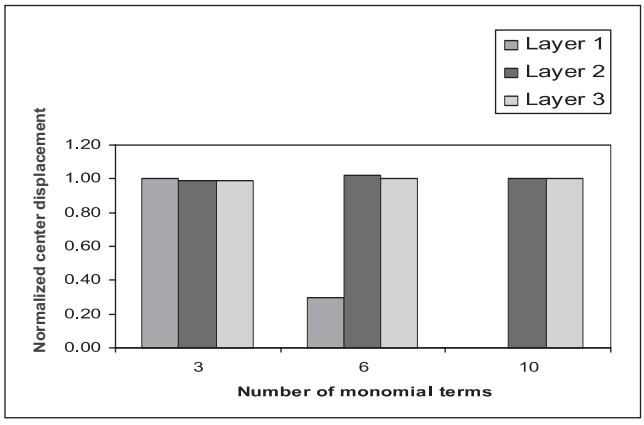

Fig. 12. CL-C thin square plate (L/D=100): normalized center displacement vs. number of monomial terms in the basis function having quadrature rule 7 x 7 for various domain of influence

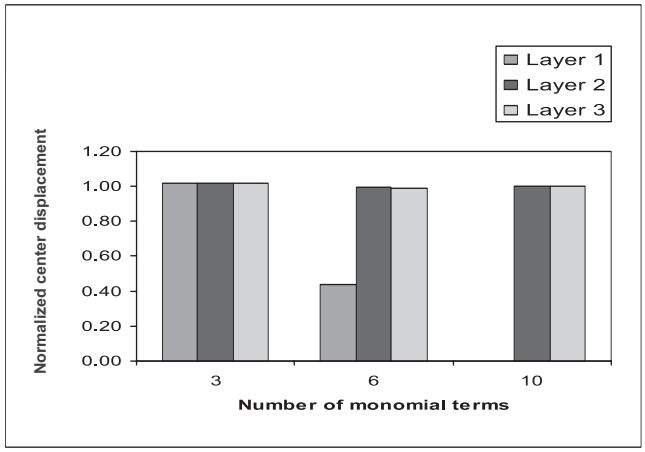

Fig. 13. CL-C thin square plate (L/D=100): normalized center displacement vs. number of monomial terms in the basis function having quadrature rule 8 x 8 for various domain of influence

Investigation of shear locking in square plates

To confirm the absence of the shear-locking phenomenon in the proposed version of EFGM, the thickness of the plate was varied. Figures 14-16 show SS-C square plate center displacement normalized with respect to thin plate solution against the length over thickness aspect ratio for domain of influence equal to 1, 2 and 3 layers respectively. While Figures 17-19 show CL-C square plate center displacement normalized with respect to thin plate solution against the length over thickness aspect ratio for domain of influence equal to 1, 2 and 3 layers respectively. Numerical results reveal that shear locking is completely eliminated for quadratic and cubic basis having DOI equal to 2 and 3 layers respectively. This also confirms that the radius of DOI must be large enough to cover n_p layers of cells surrounding the associated node, where n_p is the order of basis function, to maintain adequate numerical conditioning of system.

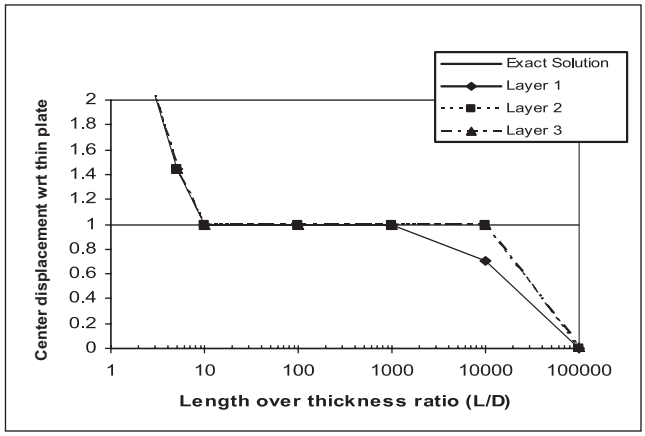

Fig. 14. SS-C square plate: normalized center displacement with respect to Kifchhoff plate solution vs. length-thickness aspect ratio for various domain of influence with linear basis

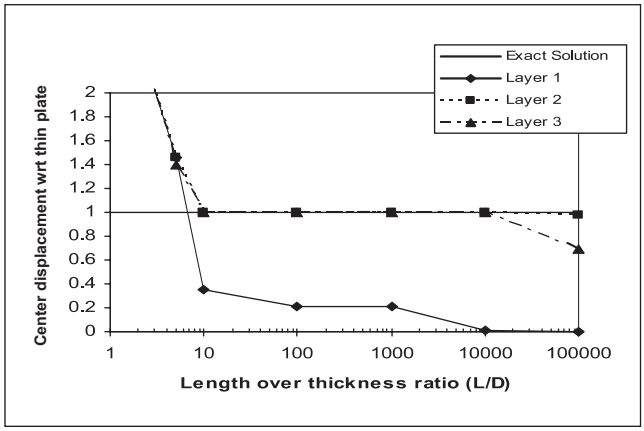

Fig. 15. SS-C square plate: normalized center displacement with respect to Kifchhoff plate solution vs. length-thickness aspect ratio for various domain of influence with quadratic basis

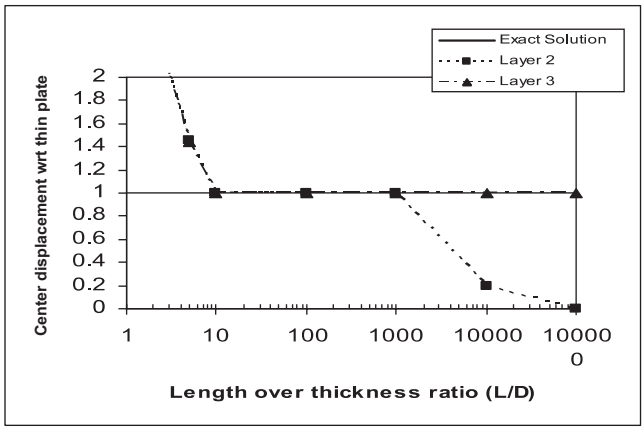

Fig. 16. SS-C square plate: normalized center displacement with respect to Kifchhoff plate solution vs. length-thickness aspect ratio for various domain of influence with cubic basis

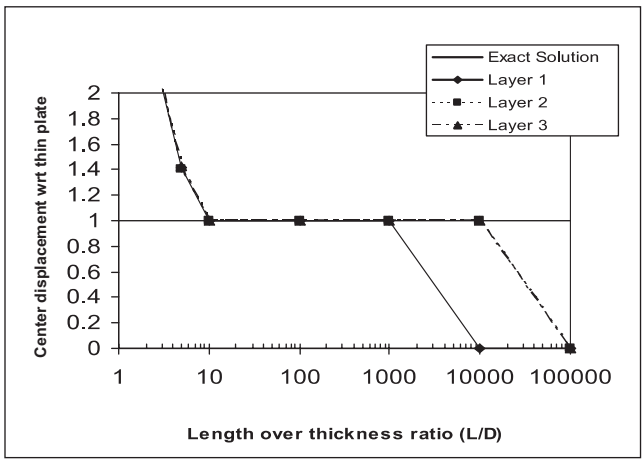

Fig. 17. CL-C square plate: normalized center displacement with respect to Kifchhoff plate solution vs. length-thickness aspect ratio for various domain of influence with linear basis

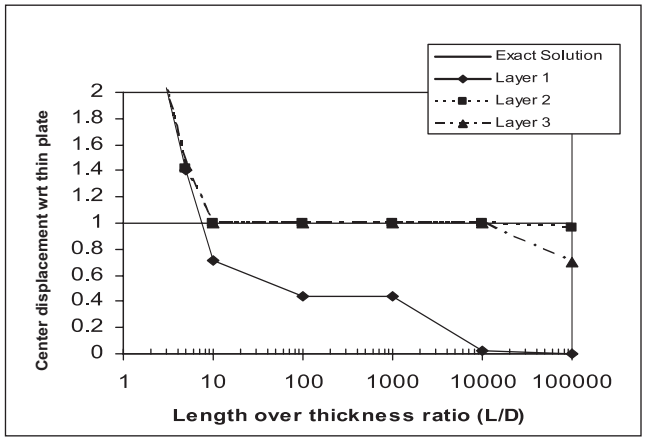

Fig. 18. CL-C square plate: normalized center displacement with respect to Kifchhoff plate solution vs. length-thickness aspect ratio for various domain of influence with quadratic basis

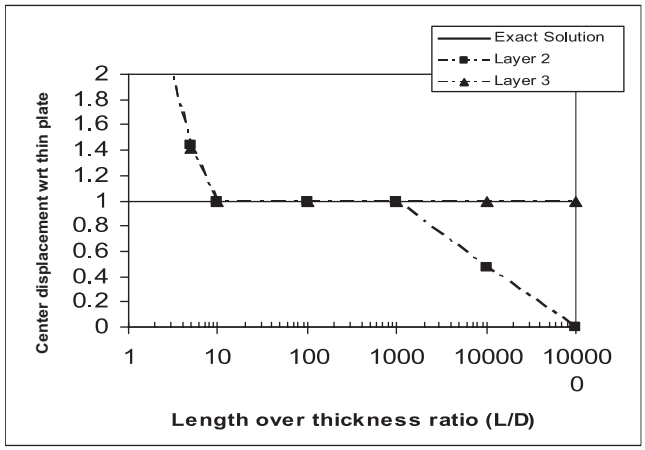

Fig. 19. CL-C square plate: normalized center displacement with respect to Kifchhoff plate solution vs. length-thickness aspect ratio for various domain of influence with cubic basis

Comparison between MK and MLS shape functions

Figures 20-21 compare the performance of MK versus the MLS shape functions, both using the quadratic basis function. It is clear that MK shape functions gives better results than MLS shape functions. It is therefore confirmed that the use of MK shape functions is superior to the use of MLS shape functions in EFGM.

Correlation parameter theta (θ)

Results in tabular format for the SS-C and CL-C cases are presented in Tables 2-3. One can observe that the correlation factor 'θ' is different for different influence layer(s).

If number of coupling nodes, *n*, is too greater than the number of basis term, *m*, as

$$n > m,$$

The smaller value of 'θ' is needed to diminish the effect of exceeding nodes which locate in the far distances. This yields the smaller of 'θ' when number of layer(s) is increased. However, if too small value of 'θ' is employed, the shape functions tend to anomalous and the solutions are inaccurate consequently.

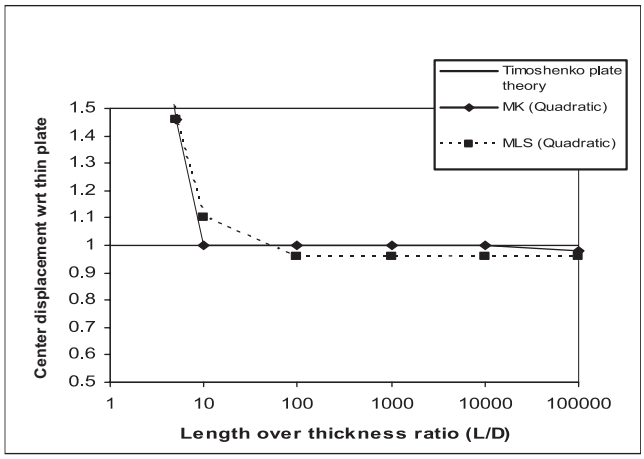

Fig. 20. SS-C square plate: normalized center displacement with respect to Kifchhoff plate solution vs. length-thickness aspect ratio

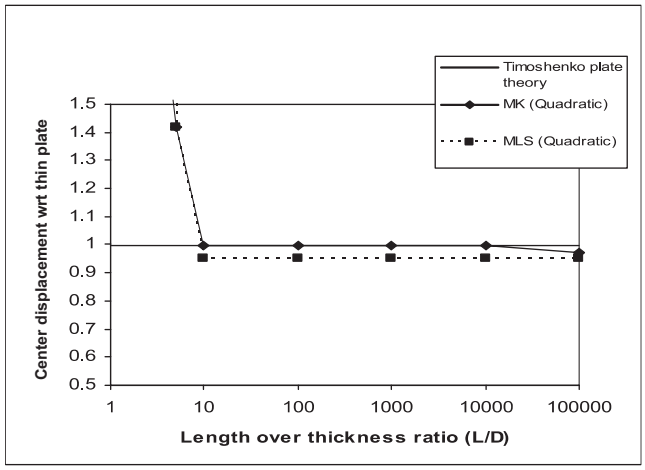

Fig. 21. CL-C square plate: normalized center displacement with respect to Kifchhoff plate solution vs. length-thickness aspect ratio

Conclusion

An improved version of the EFGM with MK shape functions is proposed in this study to address the problem of transverse shear locking in shear-deformable plates. The advantage of MK interpolation over MLS approximation in the EFGM is further confirmed. In fact with the MK interpolation, the implementation of EFGM using finite elements as integration cells can be viewed as a subclass of FEM with shape functions untied to the element structure. This study also reveals that as more coupling nodes are used, the lower value of 'θ' has to be applied to satisfy the consistency. In other words, it tends to neutralize the effect of exceeding coupling nodes to the polynomial basis component. The correlation factor theta (θ) give best results in the range 0.001-5.

Table 2. Effect of DOI in the form of Layered System on Correlation Factor Theta for SS-C

L/D	Linear Basis (3 monomial terms)			Quadratic Basis (6 monomial terms)			Cubic Basis (10 monomial terms)		
	Correlation Parameter (θ)			Correlation Parameter (θ)			Correlation Parameter (θ)		
	1 layer	2 layers	3 layers	1 layer	2 layers	3 layers	1 layer	2 layers	3 layers
3	0.2	0.2	0.05	0.4	0.2	0.1		0.4	0.09
5	1	1	0.3	0.05	0.5	0.4		0.9	0.2
10	2.4	0.74	0.55	0.01	1.1	0.5		0.1	0.58
100	7.5	0.7	0.08	3	0.9	0.5		0.5	0.08
1000	7.5	1	0.4	3	0.9	0.5		0.02	0.008
10000	10	0.01	0.007	0.05	0.004	0.004		0.001	0.005
100000	0.001	0.001	0.001	0.001	0.001	0.001		0.001	0.005

Table 3. Effect of DOI in the form of Layered System on Correlation Factor Theta for CL-C

L/D	Linear Basis (3 monomial terms)			Quadratic Basis (6 monomial terms)			Cubic Basis (10 monomial terms)		
	Correlation Parameter (θ)			Correlation Parameter (θ)			Correlation Parameter (θ)		
	1 layer	2 layers	3 layers	1 layer	2 layers	3 layers	1 layer	2 layers	3 layers
3	0.1	0.05	0.05	0.2	0.5	0.08		0.03	0.02
5	0.27	0.25	0.2	0.3	0.3	0.2		0.3	0.1
10	0.6	0.2	0.1	3	0.2	0.1		1	0.14
100	0.8	0.2	0.2	0.009	1.1	0.1		0.5	0.009
1000	0.9	0.9	0.2	0.009	0.2	0.2		0.3	0.2
10000	2	0.01	0.007	0.01	0.009	0.007		0.01	0.004
100000	0.02	0.001	0.001	0.001	0.005	0.005		0.005	0.005

REFERENCES

1. T. Belytschko, Y. Y. Lu and L. Gu, "Element-Free Galerkin Methods", *International Journal for Numerical Methods in Engineering*, Vol. 37**,** 1994, pp. 229-256.
2. L. Gu, "Moving Kriging Interpolation and Element-Fee Galerkin Method", *International Journal for Numerical Methods in Engineering*, Vol. 56, 2003, pp. 1-11.
3. P. Lancaster, K. Salkauskas, "Surfaces Generated by Moving Least Squares Methods", *Mathematics of Computation*, Vol. 37**,** 1981, pp. 141-158.
4. S. A. Memon, "Applications of Moving Kriging Shape Functions on Plate Problems", Master of Engineering Thesis, School of Civil Engineering, Asian Institute of Technology, May 2005.
5. W. Kanok-Nukulchai, P. H. Dayawans, P. Karasudhi, "An Exact Finite Element Modal for Deep Beams", *International Journal of Structures*, Vol. 1, 1981, pp. 1-7.
6. T. Belytschko, Y. Krongauz, D. Organ, M. Fleming, P. Koysl, "Meshless Methods: An Overview and Recent Developments", *Computer Methods in Applied Mechanics and Engineering*, Vol. 113, 1996, pp. 397-414.
7. B. M. Donning, W. K. Liu, "Meshless Methods for Shear-Deformable Beams and Plates", *Computer Methods in Applied Mechanics and Engineering*, Vol. 152**,** 1998, pp. 47-72.
8. K. Plengkhom, W. Kanok-Nukulchai, "An Enhancement of Finite Element Method with Moving Kriging Shape Functions", *International Journal of Computational Methods* (In press).
9. S. A. Memon, T. Akram, "On elimination of Shear Locking in Element-Free Galerkin Method Using Moving Kriging Interpolation"*, Mehran University Research Journal of Engineering & Technology*, Vol. 26, No. 1, 2007, pp. 1-10.
10. W. Kanok-Nukulchai, W. Barry, K. Saran-Yasoontorn, "Meshless formulation for shear-locking free bending element", *International Journal for Numerical Methods in Engineering*, Vol. 11**,** 2001, pp. 123-132.
11. W. Kanok-Nukulchai, W. Barry, K. Saran-Yasoontorn, P.H. Bouillard, "On elimination of shear locking in the element-free Galerkin method", *International Journal for Numerical Methods in Engineering*, Vol. 52, 2001, pp. 705-725.
12. W. Kanok-Nukulchai, W. Barry, Y. Xianpu, "An adaptive domain of influence for element-free Galerkin method", *Proceedings of the First Asian-Pacific conference on Computational Mechanics*, Sydney, Austria.